

A COMPARATIVE STUDY OF SOLID-TO-SOLID AND WET PRECIPITATION FOR THE FABRICATION OF GRAPHENE OXIDE-HYDROXYAPATITE NANOCOMPOSITE

N. C. HASHIM, D. NORDIN*

Research Centre for Sustainable Process Technology, Faculty of Engineering & Built Environment, Universiti Kebangsaan Malaysia, 43600 Bangi, Selangor, Malaysia

Graphene oxide (GO)-reinforced hydroxyapatite (HA) plays significant role in formulations applied in medicine. In this work, HA was obtained by wet chemical precipitation and GO was synthesized via a Hummer's method. GO-HA nanocomposites were prepared via two techniques, namely, solid-to-solid precipitation (Ss) and wet precipitation (Wp) methods. The morpho-structural properties of composites prepared using the two techniques with different GO contents were compared. The obtained samples were characterized by X-ray diffraction (XRD), Fourier transform infrared (FTIR), scanning electron microscopy (SEM), energy-dispersive X-ray spectroscopy, and transmission electron microscopy (TEM). FTIR, XRD, and SEM analyses showed that the GO-HA consisted mainly of HA phase. Elemental composition of oxygen of GO-HA by Ss and Wp were 34.58% and 58.69%, respectively, which confirmed the introduction of GO to HA. The average particles sizes (in width) of HA and 2.0 wt% of GO-HA by Ss and Wp were 37.28 ± 1.47 nm, 32.56 ± 1.29 nm and 32.98 ± 0.94 nm, respectively. Raman spectroscopy illustrated that there was new peak of HA in GO-HA nanocomposite. TEM analysis verified that GO was incorporated into the nanocomposite. GO-HA nanocomposites were successfully obtained via the two methods, in which the GO-HA obtained by Wp method presented a densely packed and well-defined dispersed HA onto GO nanosurface, whereas that obtained by Ss method presented randomly positioned HA particles onto GO sheets. Wp technique can be considered as a simple and convenient GO-HA fabrication technique for biocompatible implant coatings.

(Received May 6, 2019; Accepted November 6, 2019)

Keywords: Graphene oxide, Hydroxyapatite, Solid-to-solid technique, Wet precipitation technique

1. Introduction

Biomaterials research and engineering can enhance the quality and longevity of human life. Hydroxyapatite (HA) is the main constituent mineral of bones, enamel, and dentine. HA exhibits a hexagonal crystalline structure with chemical formula $\text{Ca}_{10}(\text{PO}_4)_6(\text{OH})_2$ (stoichiometry Ca/P ratio ranging from 1.5 to 2.2 compared to bone apatite) [1]. Bones contain about 65 wt% HA with needle-like shape (5–20 nm wide and 60 nm long) [2]. Mature human tooth enamel is composed by 96 wt% HA, 4 wt% organic material, and 1–6 wt% water [3].

HA bioceramic has been used for more than 30 years in biomedical application to repair bone defects [4]. In recent years, HA has gained significant interest worldwide in the fields of biomedicine and prosthetics [5]. HA does not exhibit toxic properties and can be safely used in the human body. It is also used as an implant material for filling in or reconstructing bone defects. HA is widely used in dental implants, drug carriers, scaffolds for tissue engineering, and coatings for covering the surface of implants. The biocompatibility and osteoconductivity of HA are the most important factors to their biomedical applications.

* Corresponding author: darman@ukm.edu.my

Nonetheless, HA application is restricted by its poor mechanical strength and low toughness. To improve its physicochemical properties and practicability, various modifications of HA have been applied depending on its applications, including different preparation methods (sol-gel, hydrothermal, chemical precipitation, ultrasonic-assisted, and microwave irradiation and also polymeric sponge template [6]) or HA-based composites (metals, polymer, oxides group, carbonaceous materials, and bioglasses).

Graphene oxide (GO) is suitable for hybridization with HA. It is a two-dimensional (2D) nanomaterial with high mechanical strength and biocompatibility. An improvement in mechanical strength and cytocompatibility can be achieved by combining the high strength of GO and excellent biocompatibility of HA [7] [8]. In addition, the addition of GO in HA not only improved the thermal stability of polymer but also increased the tensile strength and hardness of the composite with the increase in GO content [9]. GO/HA composites also exhibit antimicrobial characteristic [10], and can be used as drug [11] and gene delivery carriers for the cancer therapy [12]. GO/HA composites also show promising prospects for anticorrosive pigments [13] and water purification [14].

HA can be reinforced by GO through a variety of methods, such as spark plasma sintering, hydrothermal process, biomimetic mineralization, in situ chemical precipitation, simple precipitation, bioinspired mineralization [15], electrospinning, and electrophoretic nanotechnology [16].

In particular, wet precipitation method is a convenient and economic route, in which low temperature is applied ranging from 40 °C to 100 °C [16] [17], with high yield, homogenous mixing, controllable nanophase particle size [5], and low cost. Moreover, room-temperature solid-to-solid fabrication method is simple, convenience, energy-saving, environmentally friendly [19] and controllable. Compared to hydrothermal method, the reaction applies heat of up to 180 °C for 12 h, with high pressure and the use of an expensive autoclave.

The present study compared the structural and morphology properties of GO-HA nanocomposites obtained by solid-to-solid synthesis and chemical precipitation. HA was synthesized using wet chemical precipitation, whereas GO was prepared through a modified Hummer's method. GO-HA hybrid with various contents of GO were synthesized by solid-to-solid precipitation and chemical precipitation. The GO-HA nanohybrids were characterized by X-ray diffraction (XRD), Fourier transform infrared (FTIR) spectroscopy, scanning electron microscopy (SEM), energy-dispersive X-ray (EDX) spectroscopy and transmission electron microscopy (TEM) and Raman spectroscopy. This study provides basis for the development of GO-HA nanohybrid using simple, convenient, controllable, non-toxic, and environmentally friendly techniques for implant coatings.

2. Experimental

2.1. Materials

Calcium hydroxide ($\text{Ca}(\text{OH})_2$), ortho-phosphoric acid (H_3PO_4), graphite powder, sodium nitrate (NaNO_3), sulfuric acid (H_2SO_4), potassium permanganate (KMnO_4), 30% hydrogen peroxide (H_2O_2), and 5% hydrochloric acid (HCl) were obtained from Merck. Sodium hydroxide (NaOH) was purchased from R&M Chemicals. Deionised water and distilled water were used throughout this experiment.

2.2. GO Preparation

GO was synthesized using natural graphite powder through a Hummer's method [20]. Briefly, 1 g of graphite powder and 0.5 g of NaNO_3 were mixed, followed by addition of 23 mL of concentrated H_2SO_4 under constant stirring. After 1 h, the mixture was stirred in ice bath until it reached a temperature of 10 °C. Next, 4 g of KMnO_4 was slowly added under continuous stirring for 2 h while keeping the temperature at less than 10 °C to prevent overheating and explosion, and then constantly stirred at 35 °C for another 1 h. The solution was then diluted by adding 46 mL of deionised water while the reaction was heated to 90°C. After 1 h of stirring, further dilution was done using 50 mL of deionised water. To ensure complete reaction of KMnO_4 residual, 2 mL of

30% H_2O_2 was added into the mixture. The colour of mixture changed from brown to brilliant yellow. Lastly, the mixture was centrifuged and rinsed with 5% HCl aqueous solution until the pH was neutral prior freeze drying to obtain fine brown powders, designated as GO [21].

2.3. Wet precipitation of HA

$\text{Ca}(\text{OH})_2$ was used as the sole source of calcium ions. H_3PO_4 was used as source of phosphorus and NaOH as a buffering reagent to maintain the constant pH value of 10. $\text{Ca}(\text{OH})_2$ and H_3PO_4 were dissolved respectively in 100 ml of distilled water stock solution. Next, a stock of each solution was stirred constantly for 2 h, 500 rpm, and 30°C under magnetic stirring. During the synthesis, the solution of H_3PO_4 was titrated dropwise to calcium solution at 4 ml/min under continuous stirring while pH of the mixing solution was adjusted to 10 by adding NaOH solution. Afterwards, the solution was successively stirred at room temperature until completion of the reaction was indicated by the formation of thick white precipitate. The precipitate was aged overnight and washed with distilled water to remove all impurities. Next, the precipitate was filtered through a filter paper and dried at 80°C for 12 h in an oven. Finally, the sample obtained was crushed, grounded, and weighed.

2.4. Synthesis of GO-HA

2.4.1. Solid-to-solid fabrication

HA powder was dissolved in distilled water for 2 h under magnetic stirrer at 40°C . While GO powder underwent ultrasonication for 2 h. Homogenous dispersion of HA nanoparticles and 2.0 wt% of GO aqueous solution was realised in an ultrasonic bath for 5 h at room temperature. The mixture was then continuously stirred with a magnetic stirrer for 12 h at room temperature. Next, the products were left overnight, filtered, and then dried overnight in the oven at 80°C . A series of experiments were conducted under the same conditions to investigate the effects of different GO contents (0 wt%, 0.25 wt%, 0.5 wt% and 2.0 wt%) on the properties of GO-HA composites.

2.4.2. Wet precipitation

GO powder was ultrasonically dispersed in distilled water by ultrasonication for 2 h to form a stable brown GO solutions. $\text{Ca}(\text{OH})_2$ was completely dissolved in distilled water and then gradually added to the GO aqueous suspension to promote electrostatic interaction between Ca^{2+} and the negatively charged group of GO (C-O-C and OH) (

Fig. 1). The negatively charged GO surface would adsorb the positively charged calcium cations through electrostatic interaction [22], forming the homogenous $\text{GO}-\text{Ca}^{2+}$ system. The mixture was stirred for a few hours to achieve a homogenous suspension. Next, H_3PO_4 was added dropwise to above solution, and the pH was adjusted to pH 10 by adding NaOH under vigorous stirring. HA phases could precipitate out of solution with combination of PO_4^{3-} ions and Ca^{2+} [23]. The mixed solution was centrifuged and dried overnight in the oven at 80°C .

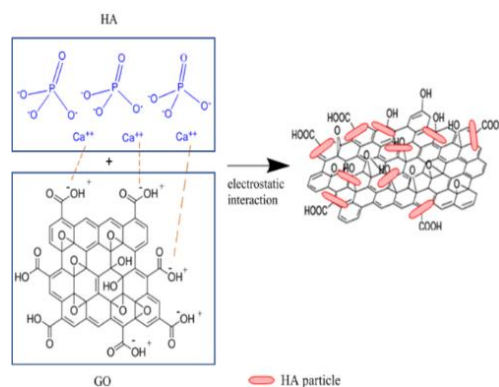


Fig. 1. Proposed interaction mechanism of GO and HA.

2.5. Characterization

The chemical composition of samples was examined by FTIR (Thermo Scientific, Nicolet 6700). The KBr pellet technique was used and the spectrum was recorded in the 400–4000 cm^{-1} region with resolution of 4 cm^{-1} . The crystal phase composition and degree of crystallisation were analysed by XRD (D8-Advance, Bruker Company, Germany) in the range $5^\circ \leq 2\theta \leq 80^\circ$ with Cu K α radiation (0.15408 nm). The surface morphological features of the samples were observed by SEM (VPSEM, LEO 1450VP) on gold-coated powder samples. EDX spectra (attached to SEM) were also obtained. TEM (Philips, TEMCM12) images of samples were obtained with an acceleration voltage 100 kV. The samples were dispersed in ethanol using ultrasonic bath and deposited (dropwise) onto carbon-coated grids. Raman spectra were recorded from 500 to 3050 cm^{-1} by Confocal Micro-Raman Imaging Spectroscopy (DXR2xi, Thermo Scientific) with excitation wavelength of 532 nm, laser power of 3.0 mV and aperture of 50 μm slit.

3. Results and discussions

3.1. FTIR Analysis

The FTIR spectra of GO, HA and GO-HA at different weight percentages (%) obtained through solid-to-solid synthesis and wet precipitation technique are shown in

Fig. 2 and

Fig. 3. The IR spectrum of GO shows broad peak at 3395.7 cm^{-1} due to OH stretching vibration of absorbed water molecules. The peak at 1727.7 cm^{-1} can be ascribed to carbonyl groups ($\text{C}=\text{O}$) on the edges of the basal planes. This spectrum also demonstrates the presence of stretching vibrations of $\text{C}=\text{C}$ at 1625.5 cm^{-1} , $\text{C}-\text{OH}$ at 1391.5 cm^{-1} and $\text{C}-\text{O}$ at 1065.8 cm^{-1} [24][25].

The FTIR spectrum of HA revealed that the broad peak (stretching vibration) at 3405.4 cm^{-1} and weak band (bending vibration) at 1642.5 cm^{-1} are attributed to the absorbed water molecules. CO_3^{2-} group was detected at 1421.9 cm^{-1} , indicating the replacement of PO_4^{3-} to CO_3^{2-} by the precipitation of HA. The spectrum also shows three bands at 1031.5 cm^{-1} , 603.0 cm^{-1} and 563.3 cm^{-1} , which represents the PO_4^{3-} group [26][27].

No remarkable difference is found between the spectra of bare HA and GO-HA composite because of only a small amount of GO is added into HA [12]. However, the carboxyl moiety peak of GO at 1730 cm^{-1} disappeared completely in GO-HA nanocomposite because of the reaction between the carboxyl moiety of GO and the calcium and phosphate moieties of HA [28], suggesting the successful introduction of GO in nanocomposite.

In addition, the $-\text{OH}$ peaks of GO-HA shifted significantly to the higher region to distinguish the amount of GO in composite. The $-\text{OH}$ peaks of solid-to-solid technique shifted from 3397.2 cm^{-1} to 3388.9 cm^{-1} and 3390.5 cm^{-1}) and (1639.2 cm^{-1} , 1645.0 cm^{-1} and 1650.8 cm^{-1}) with the increase in GO content in HA from 0.25 wt% to 0.5 wt% and 2.0 wt%. Same result is observed for the wet precipitation technique, where the $-\text{OH}$ peaks significantly increased from 3417.0 cm^{-1} to 3426.5 cm^{-1} and 3455.9 cm^{-1} and for $-\text{OH}$ peaks at (1644.2 cm^{-1} to 1647.1 cm^{-1} and 1650.8 cm^{-1}) with the increase in amount of GO in the composite. This phenomenon is due to the large amount of bulky group of OH ions over CO_3^{2-} functionalities in HA particles. The strengthened $-\text{OH}$ peaks at ~ 1640 cm^{-1} –1650 cm^{-1} is due to the stretching vibration of $\text{C}=\text{C}$ bond (1625.5 cm^{-1}) of GO [13].

The bump of curve peaks of OH group was narrower and decreased as the GO content was increased from 0.25 wt% to 2.0 wt% due to the integration of peaks of GO into HA peaks. With the increase in GO content, the characteristics absorption peaks of the sample were decreased, implying that the HA component integrated with the GO component (addition of GO into HA).

The FTIR spectra of solid-to-solid technique demonstrated that the 0.5 wt% GO-HA nanocomposite has an additional absorption band at 2361.8 cm^{-1} , attributed to P-H stretching absorption [29], and peaks of 2923.6 cm^{-1} and 2919.8 cm^{-1} , attributed to methylene group ($\text{C}=\text{H}_2$) [23][30]. The appearance of $\text{C}=\text{H}_2$ verified the existence of GO. The 2.0 wt% GO-HA

nanocomposite also has absorption peaks of P-H group at 2335.4 cm^{-1} , whereas only the P-H peaks at 2361.5 cm^{-1} of 0.5 wt% GO-HA nanocomposite was found for the wet precipitation technique. All the vibrational frequencies of the samples are summarized in Table 1.

Fig. 2 and

Fig. 3 show that the solid-to-solid and wet precipitation techniques have no obvious differences between GO-HA nanocomposites in terms of absorption profile. Nevertheless, slight differences in the spectra for the composites obtained by both techniques can be distinguished. The absorption intensity distributions of CO_3^{2-} by wet precipitation technique are clearly observed in the spectra of GO-HA nanocomposite, because $\text{Ca}(\text{OH})_2$ reacted with atmosphere oxygen during synthesis, and then transformed to CaCO_3 . The absorption peaks of CO_3^{2-} , PO_4^{3-} and OH^- groups gradually decreased with the increase in GO content in nanocomposite because the coordination interaction (C-O-C group) of Ca^{2+} is absorbed on the GO or through ion exchange with H^+ with COOH and OH groups. The absorbed Ca^{2+} then becomes nucleation sites for the following absorption of PO_4^{3-} and OH^- groups. GO not only facilitates homogenous dispersion but also provides numerous reactive sites for hybridization [31].

Table 1. Summary of vibrational frequencies observed in the FTIR spectra of composite obtained using the two techniques.

Techniques	GO content (wt%)	Vibrational modes (cm^{-1})				
		OH^-	CH_2	P-H	CO_3^{2-}	PO_4^{3-}
Solid-to-solid	0	3405.4, 1642.7	-		1421.9	1031.5, 603.0, 565.3
	0.25	3417.0, 1644.2	-	-	1416.0	1031.3, 603.1, 565.6
	0.5	3426.5, 1647.1	-	2361.5	1419.3	1031.9, 603.2, 565.5
	2.0	3455.9, 1650.8	-	-	1415.9	1031.8, 605.6, 563.1
Wet precipitation	0.25	3387.2, 1639.2, 875.2	-	-	1422.5	1035.9, 604.0, 565.1
	0.5	3388.9, 1645.0, 875.1,	2923.6, 2919.8	2361.8	1422.7	1036.3, 604.2, 565.4
	2.0	3390.5, 1650.8, 874.6	-	2335.4	1421.5	1034.1, 963.1, 604.4 564.8

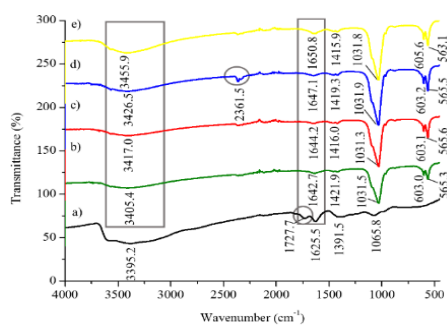


Fig. 2. FTIR spectra of a) GO b) 0.25 wt% GO-HA, c) 0.50 wt% GO-HA, d) 2.00 wt% GO-HA and e) HA obtained by solid-to-solid technique.

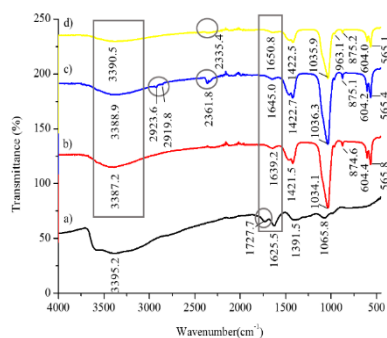


Fig. 3. FTIR spectra of a) GO b) 0.25 wt% GO-HA, c) 0.50 wt% GO-HA, d) 2.00 wt% GO-HA obtained by wet precipitation technique.

3.2. XRD Analysis

The XRD diffraction pattern in

Fig. 4 shows a comparison of graphite and GO. The sharp diffraction peak of graphite at $2\theta=26.510^\circ$ corresponds to (001) with interplanar spacing, $d=3.3595 \text{ \AA}$. GO exhibits of diffraction peak at $2\theta=10.673^\circ$ [32], which corresponds to (002) plane and an increased interplanar spacing, d , to 8.2823 \AA . The small peak at 42.037° indicates the presence of a few hexagonal graphite sheets in the GO nanosheets [12]. An increment in the distance between layers is due to the existence of oxygenated group and intercalation of water molecules during oxidation process of GO [15], [33]. Moreover, the crystallite size of GO is smaller (11.57 nm) compared to graphite (28.59nm) due to exfoliation of graphite to GO. These findings show a completed and successful exfoliation and oxidation of GO using the Hummer's method.

As shown in

Fig. 5(b) and

Fig. 6(b), the presence HA peaks indicated by hkl plane (hexagonal lattice) in the (002), (211), (112), (300), (310), (222), (213) and (004) confirm the HA samples, which matched well with the standard HA pattern (JCPDS: 064-0738). The broad peaks of HA and GO-HA nanocomposites indicate that the prepared samples were nanocrystallites [34], [35]. The XRD pattern (

Fig. 5 and

Fig. 6) of GO-HA nanocomposite had the same profile as observed in the HA nanoparticles. No GO characteristic peaks are found in the HA/GO pattern [23], [29], [36], which is due to the good dispersion of GO in HA/GO powder [28], [37]. This phenomenon could also be due to the concealing of GO peaks HA owing to lower concentration of GO than that of HA in the GO-HA composite [12][38]. On the contrary, a study by Raucci shows that the strong and sharp of (002) peaks of GO shifted and becomes sharper in the composite [35].

Meanwhile, the crystallinity of GO-HA nanocomposite gradually decreased with the increase in GO content, leading to broad diffraction peaks, which imply a decrease in intensity of diffraction peaks of GO-HA. Particularly, the intensity of the diffraction peaks of GO-HA decreased as GO content increased from 0.25 wt% to 2.0 wt%. The overall crystallinity of 0.25 wt% GO-HA, 0.5 wt% GO-HA and 2.0 wt% GO-HA were 64.7%, 62.6% and 59.7%, respectively, for solid-to-solid technique and 62.7%, 58.6% and 57.8% for wet precipitation technique. The diffracted peaks of (002) and (211) clearly show the decreasing pattern of the nanocomposites, thus suggesting the successful introduction of GO. The diffraction peaks of GO-HA nanocomposite by wet precipitation technique are sharper and higher due to the well-crystallized samples compared to that by solid-to-solid technique.

In addition, the mean crystallite size (nm) of 0.25wt% GO-HA, 0.5wt% GO-HA and 2.0wt% GO-HA were 21.62 nm, 21.83 nm and 22.12 nm, respectively, for solid-to-solid technique and 20.65 nm, 20.90 nm and 21.75 nm for wet precipitation technique. The mean

crystallite size (nm) of 0wt% GO-HA (25.97 nm) decreased due to the presence of GO. Table 2 shows the crystallinity (%) and the mean crystallite size (nm) of prepared samples at different GO contents for both techniques.

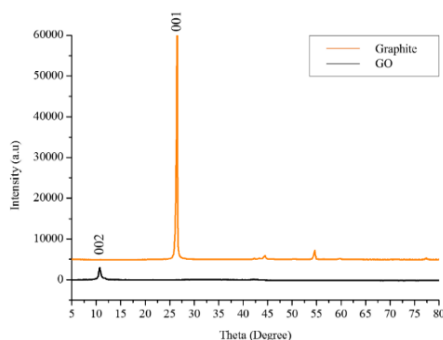


Fig. 4. XRD spectra of graphite and GO.

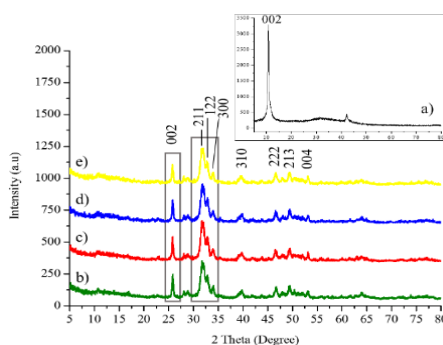


Fig. 5. XRD pattern of a) GO, b) HA, c) 0.25 wt% GO-HA d) 0.50 wt% GO-HA e) 2.00 wt% GO-HA obtained by solid-to-solid technique.

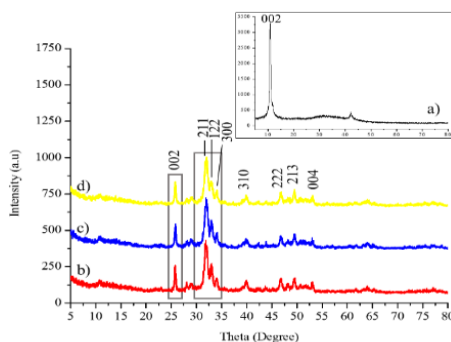


Fig. 6. XRD patterns of a) GO, b) 0.25 wt% GO-HA c) 0.50 wt% GO-HA d) 2.00 wt% GO-HA obtained by wet precipitation technique.

Table 2. Crystallinity (%) and mean crystallite size (nm) of prepared samples at different GO contents for both techniques.

Techniques	GO content (wt%)	Crystallinity (%)		Mean crystallite size (nm)
		30–35°	Overall (5–80°)	
Solid-to-solid	0	80.5	61.9	25.97
	0.25	84.7	64.7	21.62
	0.5	80.6	62.6	21.83

	2.0	77.8	59.7	22.12
Wet precipitation	0.25	80.3	62.7	20.65
	0.5	77.5	58.6	20.90
	2.0	75.2	57.8	21.75

3.3. Morphology Analysis

Fig. 7(a) shows that GO possessed a layered structure [39]. The GO nanosheets were stacked together and exhibited wrinkles on the surface of GO sheets [31]. The occurrence of wrinkles might be due to the existence of water molecules and carboxyl or hydroxyl groups [40]. GO does not have a smooth surface. Fig. 7(b) shows needle-like HA in nanoparticles size and agglomerated due to the wet precipitation technique [9] and high surface area. In the case of GO-HA nanocomposite, GO could not be recognized clearly in the SEM images (Fig. 7(c) and Fig. 7(d)), most probably due to the covering by GO sheets that were deeply immersed in HA needle-like shapes. However, the presence of GO decreased the size of HA, and a more compact structure was obtained, as supported by previous studies [23], [41]. The average particle sizes of HA as well as of 2.0 wt% of GO-HA obtained by Ss and Wp ranged from $(37.28 \pm 1.47$ nm in width), $(32.56 \pm 1.29$ nm in width) and $(32.98 \pm 0.94$ nm in width), respectively. Fig. 7, Fig. 7b and Fig. 7c show the particle size distribution (nm) of the prepared samples. The addition of GO could improve the aggregation of HA nanoparticles [36].

Furthermore, the EDX spectrum (Fig. 7) and Fig. 7)) of GO-HA nanocomposite shows the presence of Ca, P, O and C elements, which confirm the elemental composition of GO-HA nanocomposite and successful growth of HA onto the surface of GO nanosheets. By comparing both techniques, wet precipitation technique demonstrated higher oxygen element (58.69%) in nanocomposite than the solid-to-solid technique (34.58%), which confirmed the GO incorporation in the nanocomposite. These results indicated that GO contains a cluster of reactive functional groups. The high density of oxygen functional groups endowed the GO-HA with good dispersion and strong GO-HA interactions.

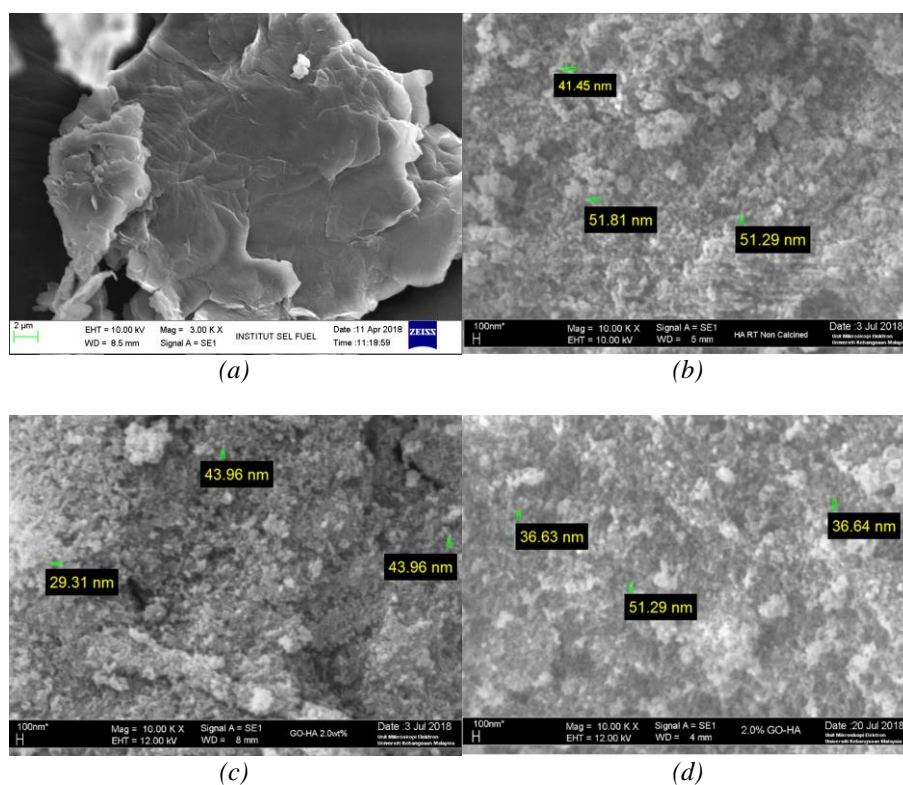


Fig. 7. SEM images of a) GO, b) HA, c) 2.00 wt% of GO-HA obtained by solid-to-solid synthesis and d) 2.00 wt% of GO-HA obtained by wet precipitation synthesis.

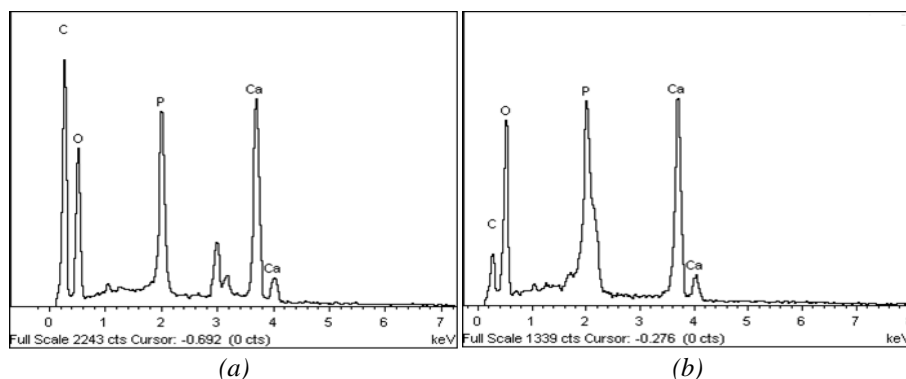


Fig. 8. EDX spectra of 2.00 wt% GO-HA obtained by a) solid-to-solid synthesis and b) wet precipitation synthesis.

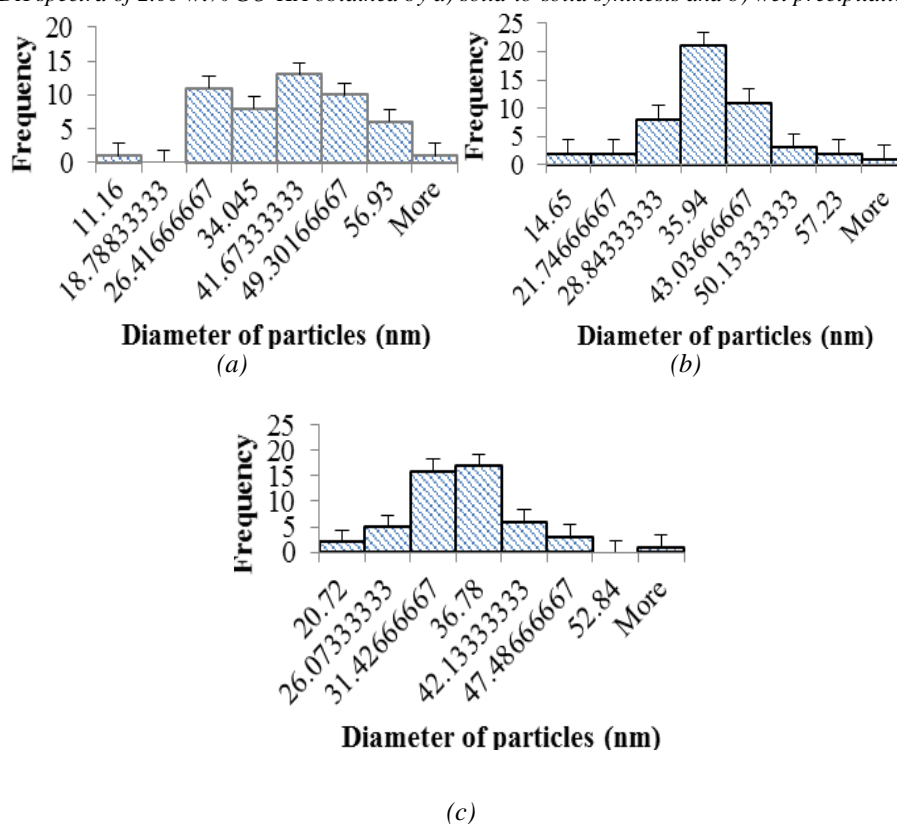


Fig. 9. Particle size distribution of a) HA, b) 2.00 wt% of GO-HA obtained by solid-to-solid synthesis, c) 2.00 wt% of GO-HA obtained by wet precipitation synthesis.

The morphologies of GO, HA and GO-HA are shown in Fig. . The TEM images show wavy wrinkles of single layer of GO sheets [42] (Fig. a). Sonication is used to expedite exfoliation process in order to obtained single layers GO in shorter time [43]. The HA nanoparticles presented typical apatite appearance of needle-like shape in nanometre scale (Fig. b).

By using wet precipitation method, the GO-HA nanocomposite was densely packed, well-defined crystalline HA nanoparticle, which are well dispersed and embedded randomly throughout the surface of the GO nanosheet (Fig. c). Moreover, the HA nanoparticles heavily occupied almost the entire surface of the GO nanosheet (Fig. d) with larger HA compared to solid-to-solid precipitation due to homogenous mixing. Meanwhile, the HA nanoparticles were randomly positioned onto GO sheets surface via the solid-to-solid technique. The HA nanoparticles are grafted onto the GO sheet through strong chemical bonding [23], [31]. GO-HA exhibits a number

of wrinkles. Nano-HA filled GO were found in layers, indicating good interaction between GO film and nano-HA [44]. The HA morphology clearly reveals the changes induced by the wet precipitation technique.

The dispersion and distribution of HA for the GO-HA nanocomposite with greater than 2.0 wt% GO cannot be seen under TEM because the GO sheets are expected to be thicker and contain abundant oxygen group. Thus, the addition of appropriate GO content is important to ensure optimal conditions for hybridization.

In situ sol-gel synthesis in [35] revealed that almost no spindle-like shape HA particles are scattered out of the matrix, suggesting a strong interaction between GO-HA and better dispersion with the increase in GO amount (1.0%, 1.5% and 2.0%). This result supports the utilization GO-HA in bone repair, bone augmentation and biomedical implants coating. Rod-like nanoparticles are intimately attached to thin layer of GO sheets through sol-gel method forming GO-HA composite for bone regeneration [45].

In [44], a hydrothermal method is used to prove that HA nanorods are randomly dispersed throughout the surface and are densely attached on the GO surface, which enhance the mechanical strength for biomedical applications. By comparison, the results obtained in the current study were almost similar yet a different and simpler technique was used, that is, fewer and less complex steps are required.

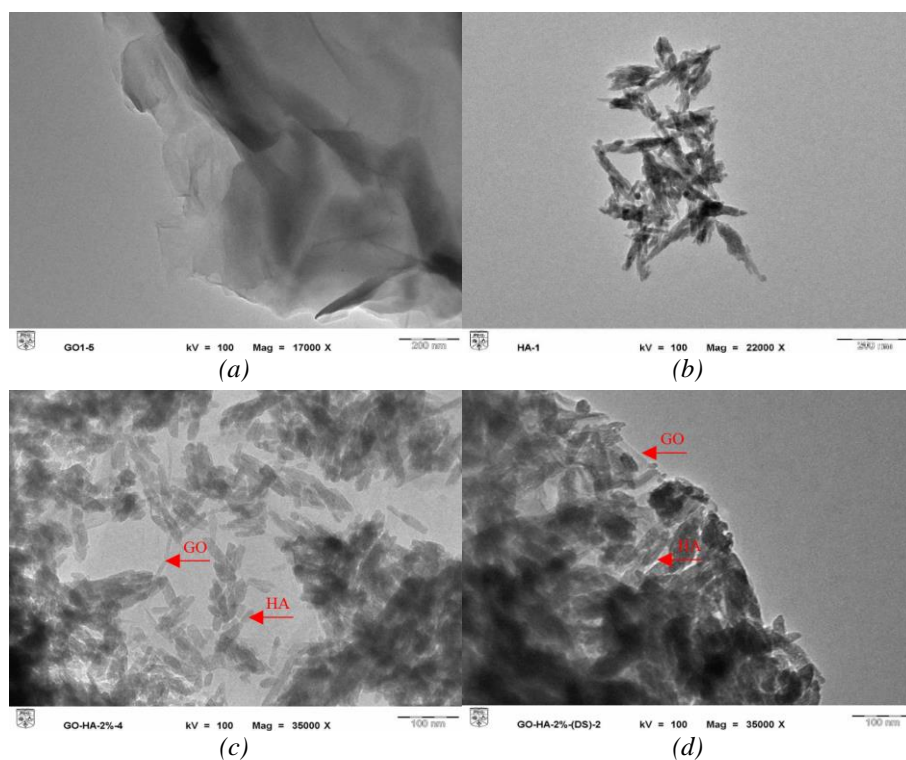


Fig. 10. TEM images of a) GO, b) HA, c) 2.00 wt% of GO-HA obtained by solid-to-solid synthesis and d) 2.00 wt% of GO-HA obtained by wet precipitation synthesis.

3.4. Raman Analysis

Raman microscopy is to determine the chemical composition or compositional changes of composites samples or individual material components about carbon-based materials. Fig. showed the results Raman spectroscopy of GO and 2.0 wt% GO-HA by wet precipitation. Raman spectra of GO indicated the characteristic of GO band around 1340.87 cm^{-1} and 1591.57 cm^{-1} , represent D and G respectively [23], [33], [39], [42], [46], [47]. The low intensity 2D band of GO at 2536.52 cm^{-1} indicating the monolayer of GO nanosheets or related to the few numbers of graphene layers were presented in the GO [39][15]. The presence of HA can be observed from the GO-HA Raman spectra. It was observed that Raman spectrum of new PO_4^{3-} bands at 957.10 cm^{-1} was very intense

and characteristic of HA [9], [23], [48] in GO-HA samples. This new band are the strongest evidence for the presence HA in GO-HA composites. Moreover, the lower intensity of D bands (1335.08 cm^{-1}) and G bands (1576.14 cm^{-1}) due to some structural transformation occurred in GO-HA [9].

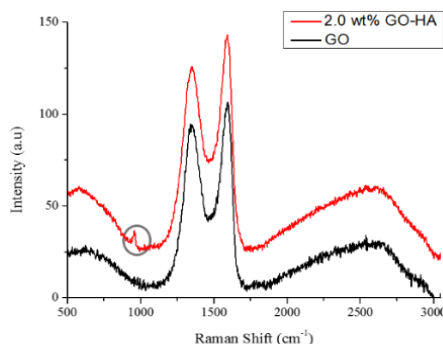


Fig. 11. Raman spectra of GO and 2.00 wt% of GO-HA obtained by wet precipitation synthesis.

4. Conclusions

Solid-to-solid precipitation (Ss) and wet precipitation (Wp) methods were applied to prepare GO-HA nanocomposites. The characteristics of the nanocomposites were compared. Both methods presented the ability to produce GO-HA hybrids with different morphologies, particle sizes and dispersity. The O compositions in GO-HA nanocomposites obtained by Ss and Wp were 34.58% and 58.69%, respectively. The overall crystallinity (%) for Ss technique of 0.25 wt% GO-HA, 0.5 wt% GO-HA, and 2.0 wt% GO-HA were 64.7%, 62.6% and 59.7% respectively, whereas 62.7%, 58.6% and 57.8%, respectively, for Wp technique. Raman spectroscopy illustrated that there was new peak of HA at 957.10 cm^{-1} in GO-HA nanocomposite. The morphology of nanocomposites was dependent on GO content and method applied. The nanocomposite containing 2.0 wt% GO obtained by Wp method exhibited more desirable morphology, compactness and dispersity than the other GO-containing HA and those obtained by the Ss method. The present study demonstrated that the Wp technique is a simpler (fewer preparation steps required) and more convenient GO-HA fabrication technique for preparing GO-HA nanocomposite implant coatings for biomedical application.

Acknowledgements

The author acknowledges the financial support by Universiti Kebangsaan Malaysia grant (GUP-2017-102). Special thanks to Dr. Darman Nordin for his encouragement and assistance.

References

- [1] M. Moldovan, D. Prodan, C. Sarosi, R. Carpa, C. Socaci, M. C. Rosu, S. Pruneanu, *Materials Chemistry and Physics*. **217**, 48 (2018).
- [2] S. Kuśnieruk, J. Wojnarowicz, A. Chodara, T. Chudoba, S. Gierlotka, W. Lojkowski, *Journal of Nanotechnology* **10**, 1586 (2016).
- [3] J. Reyes-Gasga, E. L. Martínez-Piñeiro, G. Rodríguez-Álvarez, G. E. Tiznado-Orozco, R. García-García, E. F. *Materials Science & Engineering C* (2013).
- [4] A. Binnaz, H. Yoruç, A. Aydinoglu, *Materials Science & Engineering C* (2017).
- [5] V. Dhand, K. Y. Rhee, S. Park, *Materials Science & Engineering C* **36**, 152 (2014).
- [6] J. A. Lett, M. Sundareswari, K. Ravichandran, S. Sagadevan, *Digest Journal of Nanomaterials*

- and Biostructures **13** (1), 235 (2018).
- [7] C. Chen, X. Sun, W. Pan, Y. Hou, R. Liu, X. Jiang, L. Zhang, *ACS Sustainable Chemistry and Engineering* **6** (3), 3862 (2018).
- [8] Q. Cheng, Q. Lan, C. Liu, J. Zhao, J. Liang, S. Tang, Y-C. Cao, *Interdisciplinary Journal of Chemistry* **2** (1), 1(2017).
- [9] M. Gong, Q. Zhao, L. Dai, Y. Li, T. Jiang, *Journal of Asian Ceramic Societies* **5**(2), 160 (2017).
- [10] D. Surendran, V. Baskaralingam, V. Sekar, S. Natarajan, *International Research Journal of Engineering and Technology (IRJET)* **4**, 298 (2017).
- [11] G. Bharath, B. S. Latha, E. H. Alsharaeh, P. Prakash, N. Ponpandian, *Anal. Methods* **9**(2), 240 (2017).
- [12] S. M. Prabhu, A. Khan, M. H. Farzana, C. Hwang, W. Lee, G. Lee, *Journal of Molecular Liquids*, (2018).
- [13] X. Z. Xue, J. Y. Zhang, D. Zhou, J. K. Liu, *Dyes and Pigments* **160**, 109 (2018).
- [14] H. Hosseinzadeh, S. Ramin, *International Journal of Biological Macromolecules*, (2017).
- [15] M. Ramadas, G. Bharath, N. Ponpandian, A. M. Ballamurugan, *Materials Chemistry and Physics* **99**, 179 (2017).
- [16] P. Duan, Ju. Shen, G. Zou, X. Xia, B. Jin, J. Yu, *Biomedical Materials*, 1 (2017).
- [17] M. Gong, Q. Zhao, L. Dai, Y. Li, T. Jiang, *Journal of Nanoscience and Nanotechnology* **18**(3), 1893 (2018).
- [18] A. Yelten, S. Yilmaz, *Materials Today: Proceedings* **3**(9), 2869 (2016).
- [19] D. Li, G.-Q. Zhong, Z.-X. Wu, *Journal of the Serbian Chemical Society* **80**(11), 1391 (2015).
- [20] W. S. Hummers, R. E. Offeman, *Preparation of Graphitic Oxide*, 1339 (1958).
- [21] E. Mahmoudi, L. Y. Ng, M. M. Ba-Abbad, A. W. Mohammad, *Chemical Engineering Journal* **277**, 1 (2015).
- [22] S. Peng, P. Feng, P. Wu, W. Huang, Y. Yang, W. Guo, *Nature Publishing Group*, 1 (2017).
- [23] Y. Zeng, X. Pei, S. Yang, H. Qin, H. Cai, S. Hu, L. Sui, Q. Wan, J. Wang, *Surface and Coatings Technology* **286**, 72 (2016).
- [24] P. Bansal, A. S. Panwar, D. Bahadur, *International Journal of Materials, Mechanics and Manufacturing* **2**(1), 18 (2014).
- [25] K. C. Ho, Y. H. Teow, W. L. Ang, A. W. Mohammad, *Separation and Purification Technology*, **177** (337), 2017.
- [26] F. Mohandes, M. Salavati-Niasari, M. Fathi, Z. Fereshteh, *Materials Science & Engineering C* (2014).
- [27] S. M. Mohamed Rafie, D. Nordin, *Malaysian Journal of Analytical Sciences*, **21** (1), 136 (2017).
- [28] D. Ramani, T. P. Sastry, *Cellulose* **21**, 3585 (2014).
- [29] Ö. Elif, Ö. Belma, Ş. İlkay, *Mater. Res. Express* **4**, (2017).
- [30] A. D. Dalgic, A. Z. Alshemary, *Journal of Biomaterials Applications* (2018).
- [31] Y. Bai, Y. Bai, J. Gao, W. Ma, J. Su, R. Jia, *Journal of Alloys and Compounds* (2016).
- [32] M. Fahrul, R. Hanifah, J. Jaafar, M. Aziz, A. Fauzi A, M. A. Rahman, *Jurnal Teknologi* **1**, 189 (2015).
- [33] N. 'Adilah Rosnan, T. Y. Haan, A. W. Mohammad, *Sains Malaysiana*, **47** (9), 2035 (2018).
- [34] L. T. Bang, R. Othman, *Ceramics - Silikaty* **58**(2), 157 (2014).
- [35] G. Raucci, M. D. Giugliano, A. Longo, S. Zeppetelli, G. Carotenuto, L. Ambrosio, *Journal of tissue engineering and regenerative medicine*, (2016).
- [36] M. Li, Q. Liu, Z. Jia, X. Xu, Y. Cheng, Y. Zheng, *Carbon* **67**, 185 (2014).
- [37] M. H. Bin, W. X. Su, Z. X. Tai, D. F. Sun, Y. X. Bin, B. Liu, X. Q. Ji, *Chinese Science Bulletin* **57**(23), 3051 (2012).
- [38] C. Liang, Y. Luo, G. Yang, D. Xia, L. Liu, X. Zhang, H. Wang, *Nanoscale Research Letters* **13**(15), (2018).
- [39] L. Shahriary, A. A. Athawale, *International Journal of Renewable Energy and Environmental Engineering* **2**(1), 2014.
- [40] M. Aziz, N. F. Tajul Arifin, W.-J. Lau, *Malaysian Journal of Analytical Sciences*, **23** (3), 479–487 (2019).

- [41] L. Fathyunes, J. Khalil-Allafi, S. O. R. Sheykholeslami, and M. Moosavifar, *Materials Science and Engineering C* **87**, 10 (2018).
- [42] F. Baskoro, C. Wong, S. R. Kumar, C. Chang, C. Chen, *Journal of Membrane Science* **554**, 253 (2018).
- [43] A. Rajest, M. M. Raja, S. Saha, T. Sinha, K. Gurunathan, *Advanced Science, Engineering and Medicine* **6**, 1(2014).
- [44] C. Wen, X. Zhan, X. Huang, F. Xu, L. Luo, C. Xia, *Surface & Coatings Technology*, (2017).
- [45] B. Chaudhuri, B. Mondal, D. Bhadra, S. C. Sarkar, *Chem Sci Rev Lett.* **6**(23), 1831 (2017).
- [46] K. S. S. Ku Muhamad, Mohamed. F, Radiman. S, Hamzah. A, Sarmani. S, Siong. K. K, Yasir, M. S, Rahman, I. R, MD. Rosli, N. R. A, *The 2016 UKM FST Postgraduate Colloquium* (2016)
- [47] S. Gurunathan, J. W. Han, A. A. Dayem, V. Eppakayala, J. Kim, *International Journal of Nanomedicine* **7**, (2012).
- [48] E.-S. M. Duraia, A. Hannora, Z. Mansurov, G. W. Beall, *Materials Chemistry and Physics* **132**(1), 119 (2012).